

## Article

# An Efficient Lightweight Deep-Learning Approach for Guided Lamb Wave-Based Damage Detection in Composite Structures

Jitong Ma <sup>1,\*</sup>, Mutian Hu <sup>2</sup>, Zhengyan Yang <sup>3,\*</sup>, Hongjuan Yang <sup>4</sup>, Shuyi Ma <sup>5</sup>, Hao Xu <sup>4,\*</sup>, Lei Yang <sup>4</sup>  
and Zhanjun Wu <sup>4</sup>

<sup>1</sup> College of Information Science and Technology, Dalian Maritime University, Dalian 116026, China

<sup>2</sup> School of Automation, Guangxi University of Science and Technology, Liuzhou 545000, China

<sup>3</sup> College of Transportation Engineering, Dalian Maritime University, Dalian 116026, China

<sup>4</sup> State Key Laboratory of Structural Analysis for Industrial Equipment, Dalian University of Technology, Dalian 116024, China

<sup>5</sup> School of Traffic and Electrical Engineering, Dalian University of Science and Technology, Dalian 116052, China

\* Correspondence: majitong@dmlu.edu.cn (J.M.); zyyang1993@dmlu.edu.cn (Z.Y.); xuhao@dlut.edu.cn (H.X.)

**Abstract:** Woven fabric composite structures are applied in a wide range of industrial applications. Composite structures are vulnerable to damage from working in complex conditions and environments, which threatens the safety of the in-service structure. Damage detection based on Lamb waves is one of the most promising structural health monitoring (SHM) techniques for composite materials. In this paper, based on guided Lamb waves, a lightweight deep-learning approach is proposed for identifying damaged regions in woven fabric composite structures. The designed deep neural networks are built using group convolution and depthwise separated convolution, which can reduce the parameters considerably. The input of this model is a multi-channel matrix transformed by a one-dimensional guided wave signal. In addition, channel shuffling is introduced to increase the interaction between features, and a multi-head self-attention module is designed to increase the model's global modeling capabilities. The relevant experimental results show that the proposed SHM approach can achieve a recognition accuracy of 100% after only eight epochs of training, and the proposed LCANet has only 4.10% of the parameters of contrastive SHM methods, which further validates the effectiveness and reliability of the proposed method.

**Keywords:** composite structure; structural health monitoring; damage detection; deep learning; Lamb wave; convolutional neural network



check for  
updates

**Citation:** Ma, J.; Hu, M.; Yang, Z.; Yang, H.; Ma, S.; Xu, H.; Yang, L.; Wu, Z. An Efficient Lightweight Deep-Learning Approach for Guided Lamb Wave-Based Damage Detection in Composite Structures. *Appl. Sci.* **2023**, *13*, 5022. <https://doi.org/10.3390/app13085022>

Academic Editor: Raffaele Zinno

Received: 2 March 2023

Revised: 29 March 2023

Accepted: 13 April 2023

Published: 17 April 2023



**Copyright:** © 2023 by the authors. Licensee MDPI, Basel, Switzerland. This article is an open access article distributed under the terms and conditions of the Creative Commons Attribution (CC BY) license (<https://creativecommons.org/licenses/by/4.0/>).

## 1. Introduction

Composites have attracted widespread attention and have been widely used in the fields of aviation and transportation, as they have excellent properties such as low weight, high strength, and strong flexibility [1]. Generally, a composite structure usually works under severe environments and variable conditions during its service period. Hence, hidden and diverse damages are exhibited in composite structures, making structural safety a severe challenge [2,3]. Structural health monitoring (SHM) is a promising technology that is important for ensuring structural safety, reducing maintenance costs, and extending service life [4–6]. Guided Lamb wave-based techniques are considered to be one of the most promising SHM techniques for large-scale and high-precision detection, which may propagate over long distances in large composite structures, and are also sensitive to numerous kinds of hidden damage [7,8].

In recent years, based on guided Lamb wave, many damage-detection methods have been proposed, mainly including delay-and-sum methods [9,10], phased-array methods [11], time-reversal imaging methods [12,13], and damage-probability imaging methods [14,15]. These methods can be roughly divided into two categories: physics-based (PB)

methods, and machine-learning (ML) methods. PB methods usually use prior knowledge of guided wave propagation to accurately extract useful information about damage from mixed wave signals [16–18]. However, it is difficult to quantitatively analyze the physical behavior of guided waves in complex material structures and environments. Therefore, PB methods can only be used for damage detection when the structure is well characterized and the environment is well controlled [19]. ML methods do not require prior knowledge of physical parameters and the mode of the Lamb waves [20,21]. In ML methods, by analyzing the guided wave signals before and after passing through a damage region, the damage index can be calculated and then the damage can be further detected according to the dense sensor path [22]. However, as the traditional ML method usually has a limited learning capability, it would lead to unstable results for damage detection.

With breakthroughs in the field of deep-learning techniques, it has emerged as a solution with great potential for lots of intelligent applications [23]. Deep-learning networks can automatically extract high-level features from signals and capture differences in waveforms without the requirement of any prior knowledge. Hence, deep-learning networks have been commonly used in combination with guided waves for intelligent damage detection, including artificial neural networks [22,24], deep neural networks [25], recurrent neural networks [26], autoencoder networks [27] and convolutional neural networks (CNN). The aforementioned networks have achieved a great deal in the field of SHM. Among them, CNN is the most widely used due to its advantages. For instance, Zhang et al. [28] used CNN to automatically extract the DI in the guided wave signal and output the damage-probability images to achieve damage detection of aluminum and composite plates. Miorell et al. [29] used delay and sum (DAS) to transform the guided wave signal into an image, and then CNN was adopted to predict the region of aluminum hole damage. Wang et al. [30] used CNN to establish a mapping relationship between guided wave signals and aluminum corrosion imaging that uses dispersion curves to describe the extent of the damage. Although this method has the advantage of fast imaging, it requires the usage of many sensors. Wu et al. [31] proposed an efficient Lamb wave-based damage-detection method for composite structures by integrating convolutional neural networks with continuous wavelet transform, and it has outstanding performance. Sikdar et al. [32] extracted acoustic emission damage signals from composite plates and then generated time–frequency maps by continuous wavelet transform, which were fed into CNN to identify damage regions. This method can exploit the time–frequency information in the raw signal, but it is almost unable to detect any classes. Ullah et al. [26] employed the number of frames of full wavefield propagation as input to a ConvLSTM model and the damage map as output to identify delamination damage. Although these methods are capable of accurately identifying damage, their computational complexity is rarely considered in the aforementioned methods. Their networks have high computational and memory costs, which are not conducive to industrial applications. There are two main reasons for this problem: (1) The sample size is large. The input data to the model is obtained by sampling from multiple sensors, with each sample usually consisting of several thousand elements. (2) These aforementioned SHM methods usually adopt conventional convolutional neural networks, which usually have a large number of model parameters and huge computational complexity in practice.

To address the above problem, we propose an efficient lightweight deep-learning-based damage-detection approach. In the proposed approach, first, the raw signal data are reshaped by transforming multiple one-dimensional sequences contained in one sample into a two-dimensional matrix, which can effectively reduce the size of the input data while retaining valid information and providing a new perspective for feature extraction. Then, we further propose a novel lightweight convolution and attention network (LCANet) for damage detection. In the proposed LCANet, a lightweight convolution module is designed for feature extraction using group convolution, depthwise convolution, and channel shuffle. Considering that the use of lightweight special convolution can reduce the feature-extraction capability of the model slightly and that the convolutional model

can only extract local features, a multi-head self-attention mechanism (MHSA) is further adopted in front of the fully connected layer classifier of the model to improve the model performance. Experimental results demonstrate that the proposed LCANet method can efficiently and accurately detect the damaged region with outstanding performance.

The rest of this paper is organized as follows: Section 2 introduces conventional convolutional networks for damage detection, including a brief flow of detection and the parts of a convolutional network. Our proposed approach is presented in Section 3, including the introduction of the detection system, data processing, and description of LCANet. Then, we describe the experimental setup and perform experiments on damage region recognition in Section 4. The advantages of the proposed method are demonstrated by comparison with existing methods. Finally, we conclude Section 5.

## 2. Conventional Convolutional Neural Networks

CNNs have been commonly used to detect damage to SHM in recent years. According to the form of model input, there are usually two categories of CNN-based SHM methods, which are 1D-CNN and 2D-CNN-based methods. The former method takes a one-dimensional sequence directly as input [21,33], and the last method usually takes a numerical matrix or picture as input [29,32]. In this paper, 2D-CNNs are used to extract damage features. 2D-CNNs have a great advantage of using the matrix as input compared to other damage-detection methods. First, compared to PB methods, 2D-CNN does not require any prior physical knowledge. Moreover, 2D-CNN has a more efficient feature-extraction capability than 1D-CNN through the convolution of the height and width of the sample. A basic 2D-CNN for damage region recognition mainly contains a convolutional layer, a general pooling layer, a global average pooling layer, and a fully connected layer. A conventional process for a recognition task using 2D-CNN is shown in Figure 1.

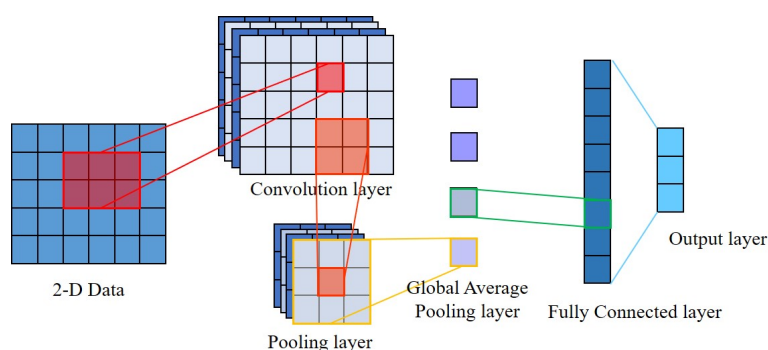


**Figure 1.** Simple process chart of 2D-CNN for damage region identification.

The convolutional layer is the heart component of CNN, which operates as shown in Figure 2a. A convolution kernel of set size slides over the input data in preset steps and computes the dot product with the covered data to achieve feature extraction. Specifically, the parameters of the convolution kernel are shared when performing the sliding convolution calculation. In conventional convolution, each input data needs to be convolved with several different convolution kernels. Therefore, the number of channels of the output features of the convolutional layer coincides with the number of convolutional kernels. The performance of the model can be improved by optimizing the size and number of convolutional kernels. In addition, the model depth can be expanded by connecting multiple convolutional layers in series to improve performance. However, it will increase the complexity of the model and the risk of overfitting. The convolution layer is usually followed by batch normalization (BN) and an activation function. The BN layer prevents gradients from disappearing or exploding and speeds up training by normalizing the current batch of data. The activation function can extract non-linear features and accelerate convergence.

The general pooling layer is shown in Figure 2b. It can reduce the feature map size and filter important information through downsampling. The pooling process may cause some

information loss. In addition, global averaging pooling (GAP) is often used in 2D-CNNs as shown in Figure 2c. GAP turns the feature map into a mean by averaging the 2D images of each channel. Feeding the mean sequence into the fully connected layer for classification will greatly reduce the parameters and the risk of overfitting.

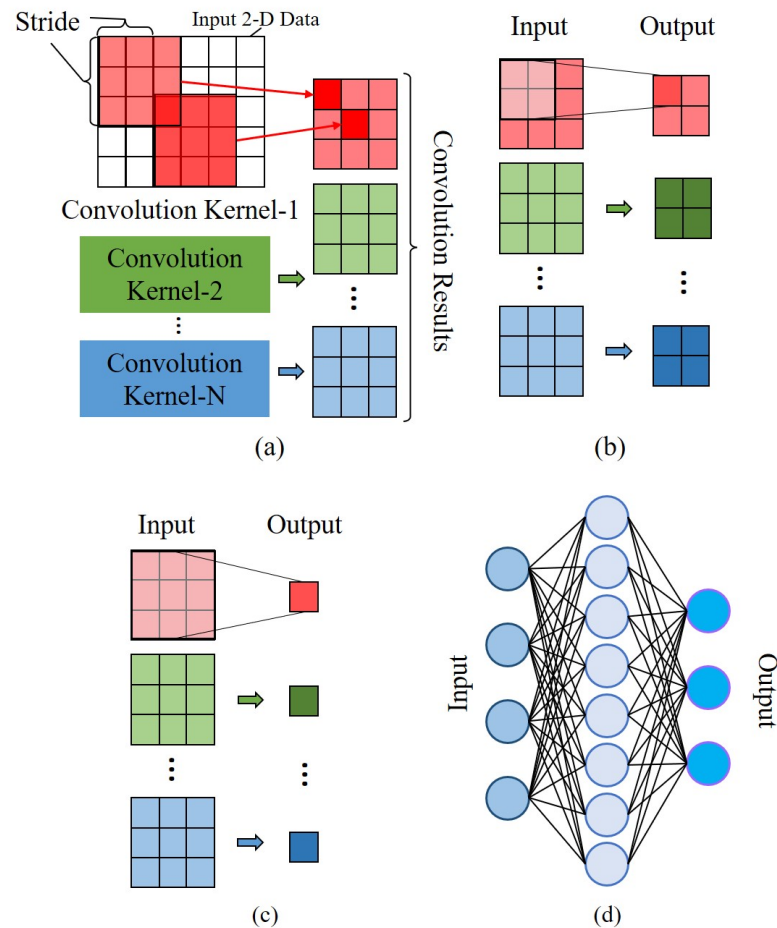


**Figure 2.** Schematic diagram of the operation process of CNN. (a) Convolution layer, (b) General pooling layer, (c) Global averaging pooling layer, (d) Fully connected layer.

After feature extraction in the convolutional layer and compression in the pooling layer, as shown in Figure 2d, the fully connected layer would perform combination and classification operations. The output of the fully connected layer is a set of numbers indicating the probability of different categories. Finally, SoftMax functions are used to filter the output of fully connected layers, and then we can obtain the most probable classification or prediction for SHM.

### 3. Proposed Method

In this section, we propose a novel efficient and lightweight damage-detection method. In the proposed method, first, time-history data obtained from a PZT sensor network would be transformed into a 2D form. Then a lightweight convolution and attention network (LCANet) is designed to perform feature extraction and damage region identification based on the transformed 2D data.

#### 3.1. Data Processing

For the data processing before LCANet, we first resample the collected time-history data as shown in Figure 3. The first half of the raw guided wave signal is highly affected by damage. Hence, we retain the first half of the one-dimensional sequence and downsample

the second half at intervals to reduce the invalid data. Then, the resampled data are transformed into three channels through the reshape operation. Transforming 1D sequences into 2D data provides a new perspective on feature extraction while retaining temporal information. Figure 3 shows the flowchart of the SHM data acquisition and process, where PZT denotes the Piezoelectric Transducer.

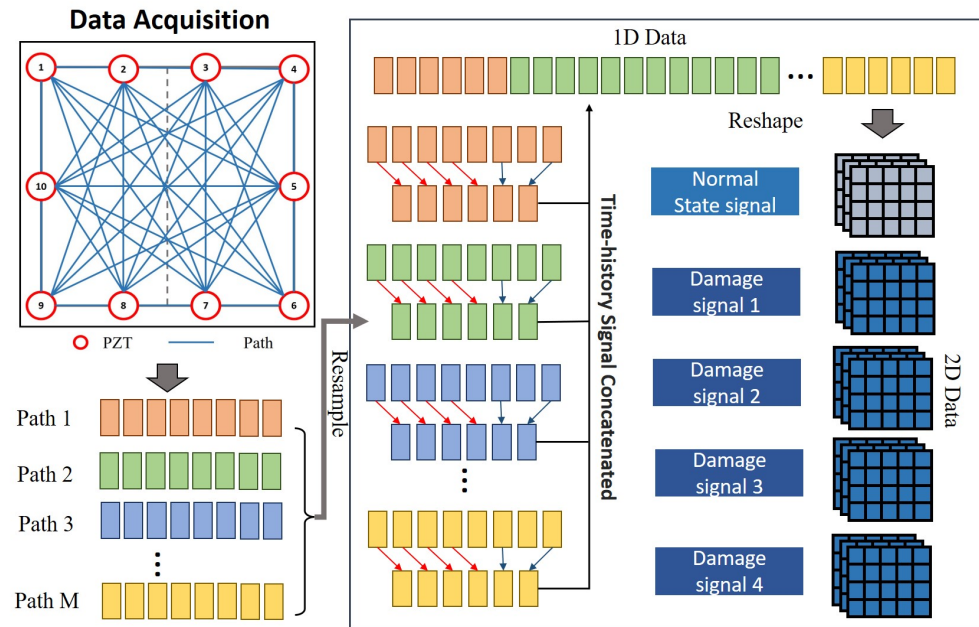


Figure 3. Flowchart of the proposed method.

### 3.2. Lightweight Convolution and Attention Network for Damage Detection

The architecture of the proposed LCANet is shown in Figure 4. The proposed LCANet mainly consists of four parts, which are the conventional convolution layer, LFE module, MHSA module, and fully connected layer. Three channels of 2D data are adopted as the input of LCANet. The conventional convolution layer performs initial feature extraction and dimensionality reduction of the data. Three LFE modules consisting of special low-computational convolutions are in tandem to extract local high-level features and further reduce the feature size. The MHSA module performs global modeling of the extracted features to obtain global contextual relationships. Finally, the extracted features are compressed by a global average pooling layer and then fed to the fully connected layer for the recognition results.

#### 3.2.1. Convolution Layer in LCANet

As shown in Figure 4, first, in the proposed LCANet, the convolution layer is mainly constructed by a 2-dimensional convolution, a batch normalization, and a ReLU activation function. We define the input data of the model as  $\mathbf{S} \in \mathbb{R}^{C_1 \times W \times H}$  and the number of output channels of the 2-dimensional convolution as  $C_2$ . Then, the convolutional layer can be represented as

$$\mathbf{F}_{CC} = \text{ReLU}(\text{BN}(\text{Conv2D}(\mathbf{S}))), \tag{1}$$

where  $\mathbf{F}_{CC} \in \mathbb{R}^{C_2 \times \frac{W}{2} \times \frac{H}{2}}$  is the output of the convolutional layer. The signal data are processed initially by the convolutional layer, with its half size and the number of expanded channels. Then,  $\mathbf{F}_{CC}$  will be fed to the LFE module for further feature extraction.

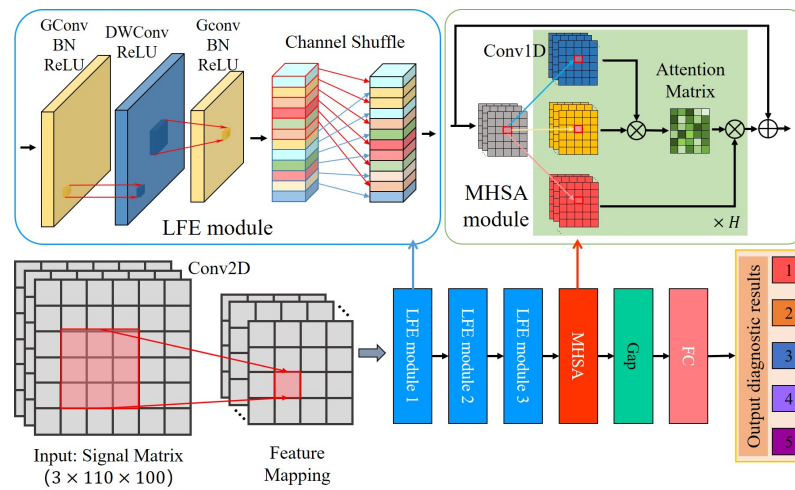


Figure 4. The architecture of LCANet for damage recognition.

### 3.2.2. Lightweight Feature-Extraction Module

As shown in Figure 4, following the convolution layer, there are three designed LFE modules, and the proposed LFE module is constructed by three main parts, which are group convolution, depthwise separable convolution, and channel shuffle. Different convolution operations are shown in Figure 5. The solid line between the input and output features represents the convolution operation. Suppose the input features are  $F_1 \in \mathbb{R}^{C_1 \times W_1 \times H_1}$ , The output features are  $F_2 \in \mathbb{R}^{C_2 \times W_2 \times H_2}$ , and only a single convolution kernel of size  $K \in \mathbb{R}^{C_2 \times k \times k}$  is used. The bias of the convolution layer is set to false. Then, the parameters of conventional convolution in Figure 5a is

$$params_{cc} = k \times k \times C_1 \times C_2 = k^2 C_1 C_2, \tag{2}$$

The floating-point operations (FLOPs) are

$$FLOPs_{cc} = (2 \times k^2 \times C_1 - 1) \times C_2 \times W_2 \times H_2 = (2k^2 C_1 - 1) C_2 W_2 H_2. \tag{3}$$

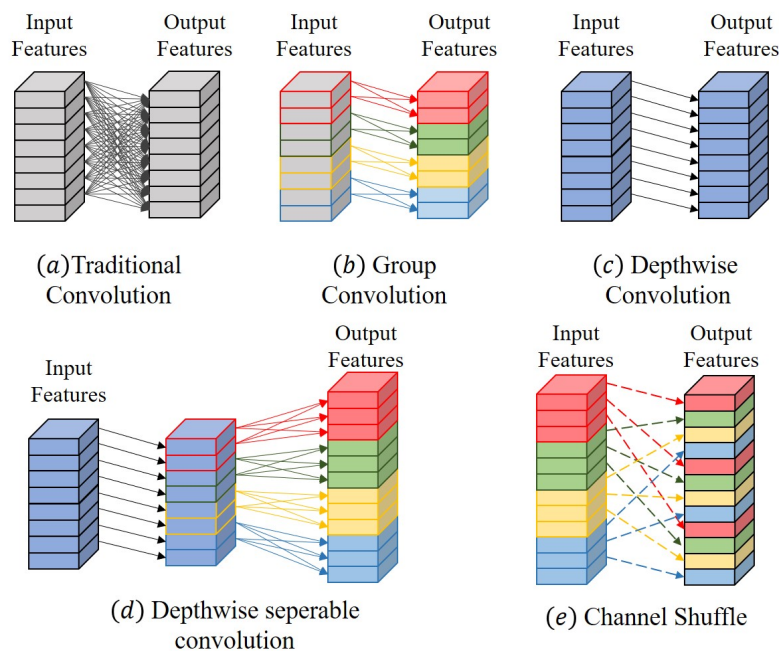


Figure 5. Mechanism of different convolution and channel shuffling.

For the group convolution in Figure 5b, the input features are divided into  $g$  groups, and the number of convolution kernels in each group is equal to the number of output channels in its group. Thus, the number of group convolution parameters is

$$params_{sgc} = k \times k \times \frac{C_1}{g} \times \frac{C_2}{g} \times g = \frac{k^2 C_1 C_2}{g}, \tag{4}$$

and its floating-point operation (FLOP) is

$$FLOPs_{sgc} = (2 \times k^2 \times \frac{C_1}{g} - 1) \times \frac{C_2}{g} \times g \times W_2 \times H_2 = (2k^2 \frac{C_1}{g} - 1) C_2 W_2 H_2, \tag{5}$$

The parameters of group convolution are  $\frac{1}{g}$  of those of conventional convolution operation. Furthermore, when the  $g$  of group convolution is equal to the number of input and output channels  $C_1 = C_2 = g$ , it would become depthwise convolution as shown in Figure 5c. The number of depthwise convolution parameters is

$$params_{dc} = k \times k \times \frac{C_1}{g} \times \frac{C_2}{g} \times g = k^2 C_1, \tag{6}$$

and

$$FLOPs_{dc} = (2 \times k^2 \times \frac{C_1}{g} - 1) \times \frac{C_2}{g} \times g \times W_2 \times H_2 = (2k^2 - 1) C_1 W_2 H_2. \tag{7}$$

The processing of features by a conventional convolution can be divided into a spatial part and a channel part. The spatial part is represented by the variation of feature map length and width, and the channel part is represented by the increase or decrease of the number of channels. Depthwise convolution and group convolution can deal with the spatial part and the channel part, respectively. Therefore, these two convolutions comprise a depthwise separable convolution that can replace the conventional convolution as shown in Figure 5d. The number of depthwise separable convolution parameters is

$$params_{dsc} = \frac{k^2 C_1 C_2}{g} + 1 \times 1 \times C_1 = \frac{k^2 C_1 C_2}{g} + C_1, \tag{8}$$

where  $1 \times 1$  is the convolution kernel for group convolution. In the proposed LFE module, we use two group convolutions and a depthwise convolution as shown in Figure 4. Moreover, the kernel of depthwise convolution is set to  $3 \times 3$  and the convolution kernel of group convolutions is set to  $1 \times 1$ . The input feature is  $F_{CC} \in \mathbb{R}^{C_1 \times W_1 \times H_1}$ , and the convolution layer can be represented as

$$F_{LC} = GConv2D(DWConv2D(GConv2D(F_{CC}))), \tag{9}$$

where  $F_{LC} \in \mathbb{R}^{C_2 \times \frac{W_1}{2} \times \frac{H_1}{2}}$  is the output of the lightweight convolution layer. In addition, although the use of group convolution can make the model lighter, but the grouping mechanism leads to the inability to communicate the channels between groups, which would further affect the network learning ability. Therefore, we add the channel shuffle after the lightweight convolution layer, and the channel shuffle is depicted in Figure 5e. Finally, the output of the LFE module can be expressed as

$$F_{LFE} = Shuffle(F_{LC}), \tag{10}$$

Specific convolution is usually used to effectively reduce the computational complexity of the feature extraction while maintaining the recognition performance of the model. In LCA Net, the LEF module is performed three times to extract more advanced features, and the feature maps are reduced, and the channels are increased at the same time.

### 3.2.3. MHSA Module

In the proposed LCANet, we use group convolution and depthwise convolution to design the LFE module by replacing the traditional convolution layers to make the model lightweight. However, the reduction of convolution operations still can affect the efficiency of feature extraction. Therefore, MHSA is further introduced to enhance the overall performance of the model by extracting global features. Then, we can obtain the local features of signal data using a conventional convolution layer and multiple LFE modules. Hence, the MHSA module can extract global contextual information based on them. As shown in Figure 4, the input features  $\mathbf{Input} \in \mathbb{R}^{C \times W_1 \times H_1}$  are divided into  $H$  groups along the channel dimension. Moreover, each group of features is generated as  $\mathbf{Q}_h, \mathbf{K}_h, \mathbf{V}_h \in \mathbb{R}^{\frac{C}{H} \times W_1 \times H_1}, 1 < h < H$  through one-dimensional convolution. The attention operation is as follows

$$\mathbf{Att}_h = \text{Softmax}\left(\frac{\mathbf{Q}_h \mathbf{K}_h^T}{\sqrt{d_k}}\right) \mathbf{V}_h, \quad (11)$$

where  $d_k$  is the dimension of the feature  $\mathbf{K}_h$  which is used to prevent excessive dot product values.  $\mathbf{Q}_h$  and  $\mathbf{K}_h$  compose an attention matrix containing global contextual information, which is multiplied by  $\mathbf{V}_h$  to realize the attention operation. The  $\mathbf{Att}_h$  is the feature map after the attention operation, which is summed along the channel dimensions to obtain the attention branch output, which is usually expressed as follows:

$$\mathbf{Att} = \text{Concat}(\mathbf{Att}_1, \dots, \mathbf{Att}_h), \quad (12)$$

where  $\text{Concat}(\cdot)$  indicates the concatenating features along the channel dimension.  $\mathbf{Att}$  and  $\mathbf{Input}$  have the same dimension and it can be obtained by summing them up at the end, which can be expressed as follows:

$$\mathbf{Out}_{MHSA} = \mathbf{Att} + \mathbf{Input}. \quad (13)$$

where  $\mathbf{Out}_{MHSA}$  is the output of the MHSA module. In the MHSA module, the correlation between different parts of the feature map can be obtained by calculating the attention weight of information at one location and other locations. In addition, the multi-head design of attention can learn different behaviors based on the same attention, which helps to capture the dependencies of signals in various ranges. Finally,  $\mathbf{Out}_{MHSA}$ , which contains local features and rich global context, will be fed into the global average pooling layer and the fully connected layer for the recognition of the damaged region.

## 4. Experimental Results and Analysis

In this section, guided wave data of composite plates are collected through real damage experiments. Furthermore, the performance of the proposed LCANet SHM method is evaluated through the comparison with existing damage-detection methods and advanced deep-learning networks.

### 4.1. Experimental Details and Guided Wave Dataset

In the experiment, a deep-learning-based damage-detection method is used to identify damaged regions in a carbon fiber composite panel. Moreover, carbon fiber composite is used as a composite material in relevant experiments. The stacking sequence of the woven fabric panel is  $[0/90]_3$ , with a whole thickness of 3 mm. The material is T700 12k carbon fiber fabric, and its mass density is  $1577.8 \text{ kg/m}^3$ . As shown in Figure 6, our experimental setup is a self-developed integrated waveguide-based SHM system, which mainly contains both hardware and software. The structural damage of the composite structure is considered in the experiments. The sound-absorbing plasticine is stuck on the composite material plate to simulate damage in the composite structure. Moreover, it generates and receives the guided wave signal at the sampling rate of 12 MHz.



**Figure 6.** Experimental setup and testbed.

The schematic of the testbed and sensor layout is shown in Figure 7. The dimensions of the composite plate testbed are (450 mm × 450 mm × 3 mm), as shown in Figure 7a. We consider an area with dimensions of (200 mm × 200 mm × 3 mm) as the region to be monitored. As shown in Figure 7a, the damage location is in the region enclosed by 10 Piezoelectric Transducers (PZTs), and in the experiments, we further divided this region into four parts for damage detection, which are D1, D2, D3, and D4. Then, the sound-absorbing plasticine is stuck on each sub-region randomly to simulate the structural damage in the composite plate, with only one damage occurring at a time. Then, the PZT sensor network is positioned on the surface of the square array damage monitoring region. This sensor network contained 10 circle-shaped PZTs and 90 propagation paths as shown in Figure 7b. Moreover, these 10 PZTs are used as both sensors and actuators. It is worth noting that when one PZT is used as an actuator/transmitter, the other PZTs are all used as receivers. The diameter of the PZT sensor is 6.25 mm and the thickness is 0.2 mm. The excitation signal is a five-cycle sinusoidal tone burst waveform modulated by a Hanning window with a center frequency of 100 kHz. The fundamental modes, both A0 and S0, are adopted at 100 kHz in the experiments. Moreover, the sampling rate is 12 MHz, as the sampling point is set as 8000, the acquired signal length is 666 μs, and the same acquired signal length is chosen for different paths. A total of 90 intact signals and 4 × 90 damaged signals are collected. Together, these samples form a dataset. In subsequent experiments, this dataset is randomly split into training and test sets in about a 7:1 ratio.

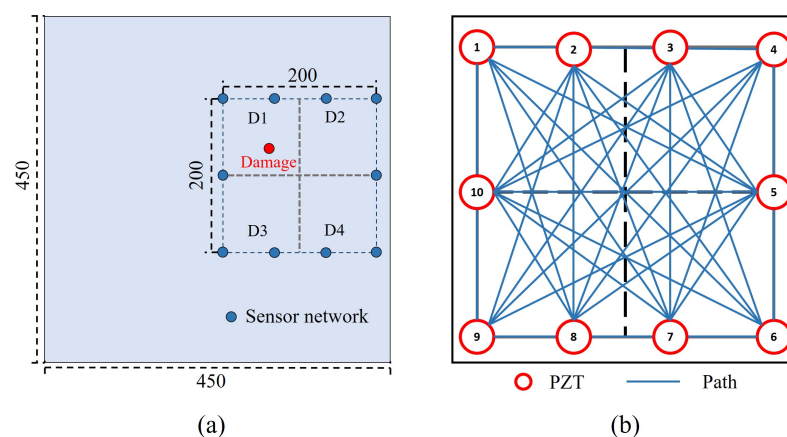


**Figure 7.** (a) Sensor arrangement in composite plate testbed; (b) Signal transmission route in composite plate testbed.

In the case of damage-simulation experiments, sound-absorbing plasticine is chosen as a medium for simulating damage due to its mechanical properties that lead to attenuation and phase shifting of guided waves. The size of the selected plasticine is about 30 mm × 30 mm × 20 mm. Moreover, Figure 8a,c illustrates the measured signals (Lamb wave) before and after attaching sound-absorbing plasticine. Furthermore, their corre-

sponding scattering signals are shown in Figure 8b,d. There are significant differences among these scattering signals.

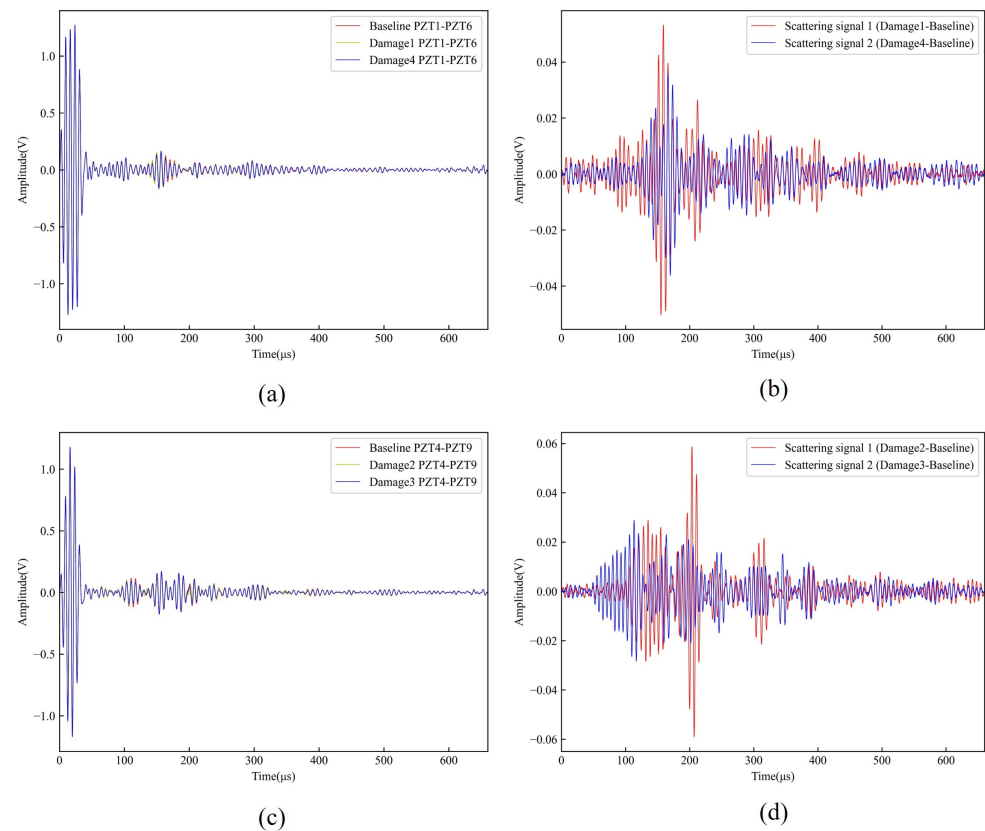


**Figure 8.** (a) Baseline wave signal and damage signals transmitted by PZT1 and received by PZT6; (b) Scattering signals corresponding to damage 1 and damage 4; (c) Baseline wave signal and damage signals transmitted by PZT4 and received by PZT9; (d) Scattering signals corresponding to damage 2 and damage 3.

Specifically, baseline signal and damage signals in different areas received by the PZT-6 and PZT-9 are shown in Figure 8, where Baseline represents the undamaged baseline Lamb wave signal and Damage1 and Damage4 denote the damage signals passing through D1 and D4 damaged area, respectively. In particular, as shown in Figure 8a, the baseline and damage signals are all transmitted by PZT-1 and received by PZT-6 before and after damage, respectively. Moreover, to further visually exhibit the differences between the baseline signal and damage signals, the scattering signals corresponding to the original signals are given in Figure 8b, which are the differences between the baseline signal and the damage signals from D1 and D4, respectively. Similarly, as shown in Figure 8c, they are baseline signal and damage signals which are transmitted by PZT-4 and received by PZT-9 passing by D2 and D3 region before and after damage, respectively. Moreover, their corresponding scattering signals are given in Figure 8d. It is apparent from Figure 8b,d that the scattered waves of the damage vary significantly from different damage areas, especially in the first few reflected/scattered waves, and there are significant differences in these different scattering signals corresponding to different damage regions. Therefore, the proposed LCANet can intelligently and efficiently extract these discriminative differences to form features for damage identification.

The experimental environment of the network model: Python3.7, PyTorch1.10, Torchvision 0.3.0, Intel(R) Core(TM) i7-6500U CPU, NVIDIA GeForce 940M GPU, 12GB memory and 932GB storage. In the training, we use the Adam optimizer with 100 epochs and the initial learning rate is set as 0.0005. The proposed LCANet is trained offline by the histori-

cally collected guided Lamb wave signals. After LCANet is well trained, it can be invoked to detect the damage from the real-time collected data. Moreover, in the experiment, we selected two damage-detection methods and a popular network as contrastive methods:

- 1D-CNN [21]: The model is built using conventional one-dimensional convolutional layers with pooling and fully connected layers, and directly using the collected 1D guided wave data as input.
- 2D-CNN [32]: The model consists of four conventional two-dimensional convolutional layers paired with pooling layers and four fully connected layers. In the experiments, the input to this model is the same as our proposed method, which is processed 2D data.
- ResNet [34]: ResNet introduces the residual structure and batch normalization between convolutional layers. This improvement solves the problem of gradient anomalies and degradation that occurs as the network deepens. In the experiments, the inputs to this model are the same as in our proposed method.

In our experiments, we use accuracy, parameters, and inference speed to evaluate the performance of the proposed model. Accuracy is the value of the number of samples judged correctly by the model as a percentage of the number of all samples. The parameters represent the total parameters of the model. The inference speed represents the time spent per sample at the time of testing.

#### 4.2. Model Performance Evaluation

In this section, we use the proposed LACNet for feature extraction and damage localization of the guided wave data. First, the model uses the training set to optimize parameters, and then to identify the damage on the test set. In this paper, the number of training epochs is set to 100.

As shown in Figure 9, the loss of the proposed LACNet is gradually decreasing with the increase of training epochs. The loss decreases rapidly when the epoch is less than 10 and then remains stable. It indicates that the model has converged after repeated learning.

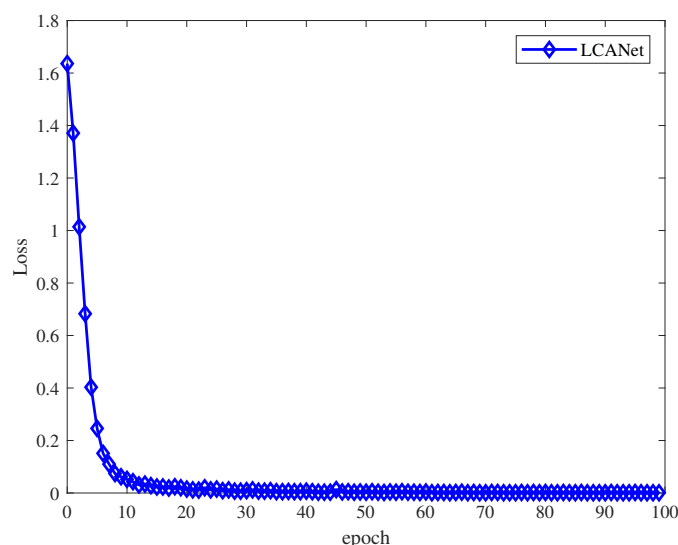


**Figure 9.** Training loss of LACNet.

Furthermore, as shown in Figure 10, it is the accuracy variation between the proposed model and the contrastive models during the training process. It is obvious in Figure 9 that LACNet is better than other contrastive models. LACNet does not learn enough during the first few training sessions, so the accuracy was only 20%. However, after the sixth training stage, the accuracy rate improved significantly. After only eight training stages, the accuracy rate reached 100%. This shows that LACNet has a powerful feature extraction and learning capability. In particular, the loss is not minimized at this point, but the damage is accurately identified. The 2D-CNN-based SHM methods also have superior performance,

followed by ResNet, which both use 2D data as input. ResNet accuracy is slow to improve, because the model was too deep while the training samples are few. Moreover, it also affects the speed of learning. 1D-CNN required at least 40 iterations for accurate recognition and the rate of increase in accuracy is also slow. Therefore, compared with other SHM contrastive methods, the proposed LCANet has outstanding performance.

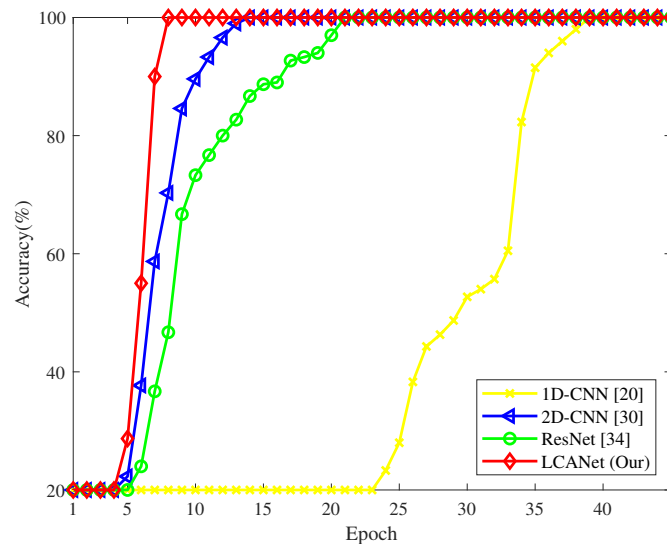


Figure 10. Accuracy of damaged area detection using LACNet and contrast models.

### 4.3. Ablation Study

The ablation study of LCANet is performed to further evaluate the effectiveness of channel shuffling and MHSA. In this experiment, we denote the LCANet model with channel shuffling and MHSA removed as CNN, the model with channel shuffling only removed as CNN+MHSA, and the model with MHSA only removed as CNN+Shuffle.

The results of the ablation experiments are shown in Figure 11. Compared with CNN, CNN+Shuffle can improve accuracy with fewer epochs, but it does not speed up the process of complete recognition. This is reasonable as channel shuffle works to increase data interaction between channels to avoid model mislearning, rather than directly contributing to learning speed. In contrast to channel shuffling, the number of cycles required for model training is reduced after using MHSA. This is because the MHSA brings additional global information that makes the various categories of samples more distinguishable.

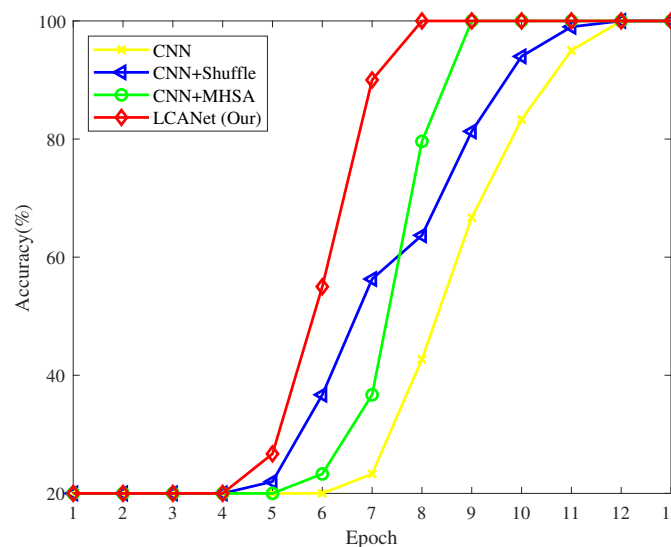
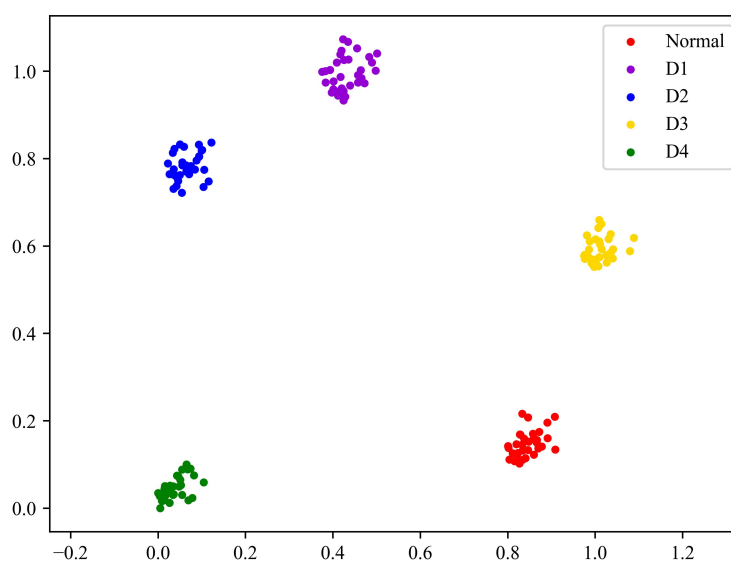


Figure 11. Ablation study of LACNet.

The ablation experiments proved that both channel shuffling and MHSA in LACNet are effective, allowing for faster and more stable model training.

#### 4.4. Visualization of Feature Maps

In this subsection, we use principal component analysis (PCA) to visualize feature maps to present the recognition results more intuitively. We extract the fully connected layer output feature maps of LACNet as input to the PCA method. PCA outputs two-dimensional data by the dimension reduction process. The visualization results of the feature map are shown in Figure 12, where Normal indicates the normal state and D1–D4 are samples with different areas of damage. The same classes of samples converge into clusters. It indicates that the differences between all kinds of samples are obvious and there is no confusion in the recognition of damage in the composite structure. Hence, the proposed method has a superior performance.



**Figure 12.** Visualization of model output.

#### 4.5. Computational Complexity

We further evaluate the proposed model by comparing it with other contrastive methods. We compare different models in terms of parameters, epochs, and inference time.

As shown in Table 1, the proposed LCANet SHM method has the highest accuracy among other contrastive methods in damage identification. In terms of parameters, 1D-CNN has more than 1.44 million parameters, which use one-dimensional sequences as model inputs. 2D-CNN has more than 23.15 million parameters, which is the highest among the four models. As two-dimensional convolution operation requires far more parameters than one-dimensional convolution, 2D-CNN has more parameters using two-dimensional data as input. The ResNet designed with the residual structure has 11.37 million more parameters, which is about half of the 2D-CNN. However, the proposed LACNet only has 59,285 parameters, less than 1/24 of that of 1D-CNN. In addition, LACNet requires only eight training sessions for accurate recognition, while 1D-CNN requires at least 40 sessions to reach the same recognition level. This is because one-dimensional convolution filters have limited coverage and poor feature-extraction ability for longer sequences. In terms of inference speed, LCANet is much faster than 2D-CNN and ResNet, but a little slower than 2D-CNN. There are two reasons for this: First, the use of group convolution and depthwise convolution can be used to effectively reduce model parameters. However, it has a reduced feature-extraction capability and requires more channels to improve performance. In general, the inference speed of LCANet is acceptable. Having only trained eight epochs,

the proposed LACNet method can reach 100% recognition accuracy, which is 80%, 29.7%, and 53.3% higher than 1D-CNN, 2D-CNN, and ResNet, respectively.

**Table 1.** Computational Complexity Comparison of Different SHM Methods.

Methods	Parameters	Epochs	Inference Time (ms/Sample)	Accuracy at 8 Epoch (%)
1D-CNN	1,446,453	40	101	20
2D-CNN	23,155,757	14	21.3	70.3
ResNet	11,378,821	21	228.6	46.7
<b>LACNet (Our)</b>	<b>59,285</b>	<b>8</b>	<b>33.9</b>	<b>100</b>

In summary, the proposed SHM method is an effective and efficient method for damage detection in a composite structure.

## 5. Conclusions

In this paper, we proposed a novel efficient and lightweight approach for damage recognition in a composite structure. In the proposed method, first, a one-dimensional signal is transformed into two-dimensional data, which not only reduces the sample size but also provides a new perspective for information extraction. Then, a lightweight network is designed to deal with the samples through special convolution. Specifically, we designed a novel convolution layer, which mainly consists of group convolution and depthwise convolution, to perform feature extraction. The designed lightweight model is of great importance for the deployment and application of damage-detection systems. In addition, a multi-head self-attention module is introduced to take advantage of its unlimited effective receptive fields to obtain global contextual information. Differences between the various types of samples are more easily explored using local and global fusion features. Relevant experiments are conducted to verify the effectiveness of the proposed method. More lightweight models to achieve precise identification of damage in complex conditions or environments is the future direction of this research.

**Author Contributions:** Conceptualization, J.M., M.H. and Z.Y.; methodology, J.M., M.H. and Z.Y.; software, S.M.; validation, H.Y., S.M., H.X. and L.Y.; resources, S.M. and H.X.; writing—original draft preparation, J.M. and M.H.; writing—review and editing, J.M., M.H. and Z.Y.; supervision, Z.W.; funding acquisition, J.M. and Z.W. All authors have read and agreed to the published version of the manuscript.

**Funding:** This work was supported by the National Natural Science Foundation of China under Grant no. 62101090 and 12102075, the China Postdoctoral Science Foundation with Grant no. 2021M700656 and no. 2022M720629, the the Fundamental Research Funds for the Central Universities under Grant 3132022229, and the Natural Science Foundation of Liaoning Province of China (No. 2022-MS-422), and the Science and Technology Research Project of Liaoning Provincial Department of Education (No. LJKMZ20221908).

**Institutional Review Board Statement:** Not applicable.

**Informed Consent Statement:** Not applicable.

**Data Availability Statement:** The data presented in this study are available on request from the corresponding author.

**Conflicts of Interest:** The authors declare no conflict of interest.

## References

- Zhang, Z.; Liu, M.; Li, Q.; Ang, Y. Visualized characterization of diversified defects in thick aerospace composites using ultrasonic B-scan. *Compos. Commun.* **2020**, *20*, 100435. [[CrossRef](#)]
- Liu, B.; Hong, X.; Yang, B. Grain refinement and localized amorphization of additively manufactured high-entropy alloy matrix composites reinforced by nano ceramic particles via selective-laser-melting/remelting. *Compos. Commun.* **2020**, *19*, 56–60. [[CrossRef](#)]

3. Ma, J.; Qiu, T.; Tian, Q. Fast blind equalization using bounded non-linear function with non-Gaussian noise. *IEEE Commun. Lett.* **2020**, *24*, 1812–1815. [[CrossRef](#)]
4. Zhou, P.; Yang, X.; Su, Y.; Yang, J.; Xu, L.; Wang, K.; Zhou, L.M.; Su, Z. Direct-write nanocomposite sensor array for ultrasonic imaging of composites. *Compos. Commun.* **2021**, *28*, 100937. [[CrossRef](#)]
5. Ma, J.; Liu, H.; Peng, C.; Qiu, T. Unauthorized broadcasting identification: A deep LSTM recurrent learning approach. *IEEE Trans. Instrum. Meas.* **2020**, *69*, 5981–5983. [[CrossRef](#)]
6. Su, Y.; Xu, L.; Zhou, P.; Yang, J.; Wang, K.; Zhou, L.M.; Su, Z. Carbon nanotube-decorated glass fibre bundles for cure self-monitoring and load self-sensing of FRPs. *Compos. Commun.* **2021**, *27*, 100899. [[CrossRef](#)]
7. Yang, X.; Wang, K.; Zhou, P.; Xu, L.; Su, Z. Imaging damage in plate waveguides using frequency-domain multiple signal classification (F-MUSIC). *Ultrasonics* **2022**, *119*, 106607. [[CrossRef](#)]
8. Yang, Z.; Yang, L.; Zhang, J.; Ma, S.; Tian, T.; Deng, D.; Wu, Z. Damage shape recognition algorithm of composite woven fabric plate based on guided waves. *Compos. Struct.* **2023**, *303*, 116351.
9. Vishnuvardhan, J.; Muralidharan, A.; Krishnamurthy, C.V.; Balasubramaniam, K. Structural health monitoring of anisotropic plates using ultrasonic guided wave STMR array patches. *NDT E Int.* **2009**, *42*, 193–198. [[CrossRef](#)]
10. Ma, J.; Zhang, J.; Yang, Z.; Liu, H.; Wan, L.; Qiu, T. Super-resolution time delay estimation using exponential kernel correlation in impulsive noise and multipath environments. *Digit. Signal Process.* **2023**, *133*, 103882. [[CrossRef](#)]
11. Rajagopalan, J.; Balasubramaniam, A.; Krishnamurthy, C. A phase reconstruction algorithm for Lamb wave based structural health monitoring of anisotropic multilayered composite plates. *J. Acoust. Soc. Am.* **2006**, *119*, 872–878. [[CrossRef](#)]
12. Leleux, A.; Micheau, P.; Castaigns, M. Long Range Detection of Defects in Composite Plates Using Lamb Waves Generated and Detected by Ultrasonic Phased Array Probes. *J. Nondestruct. Eval.* **2013**, *32*, 200–214. [[CrossRef](#)]
13. He, J.; Yuan, F.-G. Damage identification for composite structures using a cross-correlation reverse-time migration technique. *Struct. Health Monit.* **2015**, *14*, 558–570. [[CrossRef](#)]
14. He, J.; Yuan, F.-G. A quantitative damage imaging technique based on enhanced CCRTM for composite plates using 2D scan. *Smart Mater. Struct.* **2016**, *70*, 105022. [[CrossRef](#)]
15. Hay, T.R.; Royer, R.L.; Gao, H.; Zhao, X.; Rose, J.L. A comparison of embedded sensor Lamb wave ultrasonic tomography approaches for material loss detection. *Smart Mater. Struct.* **2006**, *15*, 946. [[CrossRef](#)]
16. Wang, Y.; Gao, L.; Yuan, S.; Qiu, L.; Qing, X. An adaptive filter-based temperature compensation technique for structural health monitoring. *J. Intell. Mater. Syst. Struct.* **2014**, *25*, 2187–2198. [[CrossRef](#)]
17. Sun, H.; Shao, W.; Song, J.; Yang, X.; Wang, Y.; Qing, X. Lamb wavefield-based monogenic signal processing for quantifying delamination in composite laminates. *Smart Mater. Struct.* **2022**, *31*, 105030. [[CrossRef](#)]
18. Liu, X.; Yu, Y.; Lomov, S.V.; Wang, Y.; Qing, X. The numerical and experimental investigations for the curing monitoring of woven composites with Lamb waves. *Measurement* **2022**, *200*, 111604. [[CrossRef](#)]
19. Jin, H.; Yan, J.; Liu, X.; Li, W.; Qing, X. Quantitative defect inspection in the curved composite structure using the modified probabilistic tomography algorithm and fusion of damage index. *Ultrasonics* **2021**, *113*, 106358. [[CrossRef](#)]
20. Zhang, B.; Hong, X.; Liu, Y. Distribution adaptation deep transfer learning method for cross-structure health monitoring using guided waves. *Struct. Health Monit.* **2022**, *21*, 853–871. [[CrossRef](#)]
21. Shao, W.; Sun, H.; Wang, Y.; Qing, X. A multi-level damage classification technique of aircraft plate structures using Lamb wave-based deep transfer learning network. *Smart Mater. Struct.* **2022**, *31*, 075019. [[CrossRef](#)]
22. Peretto, D.; De Luca, A.; Peretto, M.; Lamanna, G.; Caputo, F. Damage Detection in Flat Panels by Guided Waves Based Artificial Neural Network Trained through Finite Element Method. *Materials* **2021**, *14*, 7602. [[CrossRef](#)] [[PubMed](#)]
23. Cantero-Chinchilla, S.; Wilcox, P.D.; Croxford, A.J. Deep learning in automated ultrasonic NDE—developments, axioms and opportunities. *NDT E Int.* **2022**, 102703. [[CrossRef](#)]
24. Feng, B.; Pasadas, D.J.; Ribeiro, A.L.; Ramos, H.G. Locating defects in anisotropic CFRP plates using ToF-based probability matrix and neural networks. *IEEE Trans. Instrum. Meas.* **2019**, *68*, 1252–1260. [[CrossRef](#)]
25. Humer, C.; Höll, S.; RKralovec, C.; Schagerl, M. Damage identification using wave damage interaction coefficients predicted by deep neural networks. *Ultrasonics* **2022**, *124*, 106743. [[CrossRef](#)] [[PubMed](#)]
26. Ullah, S.; Ijjeh, S.A.; Kudela, P. Deep learning approach for delamination identification using animation of Lamb waves. *Eng. Appl. Artif. Intell.* **2023**, *117*, 105520. [[CrossRef](#)]
27. Yu, Y.; Liu, X.; Wang, Y.; Wang, Y.; Qing, X. Lamb wave-based damage imaging of CFRP composite structures using autoencoder and delay-and-sum. *Compos. Struct.* **2022**, *303*, 116263. [[CrossRef](#)]
28. Zhang, B.; Hong, X.; Liu, Y. Deep convolutional neural network probability imaging for plate structural health monitoring using guided waves. *IEEE Trans. Instrum. Meas.* **2021**, *70*, 1–10. [[CrossRef](#)]
29. Miorelli, R.; Fisher, C.; Kulakovskiy, A.; Chapuis, B.; Mesnil, O.; D’Almeida, O. Defect sizing in guided wave imaging structural health monitoring using convolutional neural networks. *NDT E Int.* **2021**, *122*, 102480. [[CrossRef](#)]
30. Wang, X.; Li, J.; Wang, D.; Huang, X.; Liang, L.; Tang, Z.; Fan, Z.; Liu, Y. Sparse ultrasonic guided wave imaging with compressive sensing and deep learning. *Mech. Syst. Signal Process.* **2022**, *178*, 109346. [[CrossRef](#)]
31. Wu, J.; Xu, X.; Liu, C.; Deng, C.; Shao, X. Lamb wave-based damage detection of composite structures using deep convolutional neural network and continuous wavelet transform. *Compos. Struct.* **2021**, *276*, 114590. [[CrossRef](#)]

32. Sikdar, S.; Liu, D.; Kundu, A. Acoustic emission data based deep learning approach for classification and detection of damage-sources in a composite panel. *Compos. Part B Eng.* **2022**, *228*, 109450. [[CrossRef](#)]
33. Ma, J.; Hu, M.; Wang, T.; Yang, Z.; Wan, L.; Qiu, T. Automatic Modulation Classification in Impulsive Noise: Hyperbolic-Tangent Cyclic Spectrum and Multibranch Attention Shuffle Network. *IEEE Trans. Instrum. Meas.* **2023**, *72*, 1–13. [[CrossRef](#)]
34. Ma, J.; Lin, S.-C.; Gao, H.; Qiu, T. Automatic Modulation Classification Under Non-Gaussian Noise: A Deep Residual Learning Approach. In Proceedings of the IEEE International Conference on Communications (ICC), Shanghai, China, 20–24 May 2019; pp. 1–6.

**Disclaimer/Publisher’s Note:** The statements, opinions and data contained in all publications are solely those of the individual author(s) and contributor(s) and not of MDPI and/or the editor(s). MDPI and/or the editor(s) disclaim responsibility for any injury to people or property resulting from any ideas, methods, instructions or products referred to in the content.